Pure Appl. Geophys. 178 (2021), 39–54

https://doi.org/10.1007/s00024-020-02643-5

Pure and Applied Geophysics

Slip Rates and Seismic Potential Along Main Faults in the Eastern Mediterranean and Caucasus from dense GPS Observations and Seismic Data

Bahruz Ahadov[1,2,3,4] and Shuanggen Jin[1]

Abstract—The Eastern Mediterranean and Caucasus regions are two of the most seismically active deforming continental regions. Monitoring and studies of the extensive deformation processes in this comparatively limited region enhance our understanding of the continental collision in the region. In this paper, we built a new elastic block model to constrain present-day plate motions and regional deformation in the intraplate zone and estimate fault slip rates from a dense global positioning system (GPS) velocity field. We additionally considered differences in moment accumulation rate per unit fault length using seismogenic and geodetic depth along the main faults. The right-lateral slip rates were estimated at between 24.33 ± 0.47 and 28 ± 0.5 mm/year along the North Anatolian Fault Zone (NAFZ) and the left-lateral slip at 10.6 ± 0.9 to 12 ± 1 mm/year on the East Anatolian Fault Zone (EAFZ). The Dead Sea Transform Fault (DSTF) slip rate ranges between 4.1 ± 0.95 and 6 ± 1 mm/year. The slip rate for the Main Caucasus Thrust Fault (MCTF) is 6.5 ± 0.2 to 14.3 ± 0.7 mm/year from west to the east. A shallow locking depth of 9 ± 3.2 km was found in the Marmara region. The locking depth along the DSTF is 10.9 ± 5.5 km in the northern segment, 9 ± 6.7 km in the central section and 11.8 ± 4 km in the southern section. The locking depth of the EAFZ is 16.7 ± 4.4 km in the northern segment, 19.8 ± 7.4 km in the middle segment and 12.5 ± 4.2 km in the southern segment. The locking depths along the MCTF range between 12.7 ± 5.8 and 17.8 ± 4.9 km from west to east. Our new block model has the best fit to the observed velocities. The results provide an overall understanding of fault activity and have implications for the earthquake hazard along the main faults in the region.

Keywords: Block model, slip rate, seismic potential, GPS, Eastern Mediterranean, Caucasus.

Abbreviations

GPS	Global positioning system
CGPS	Continuous global positioning system
SGPS	Survey-mode global positioning system
NAFZ	North Anatolian Fault Zone
EAFZ	East Anatolian Fault Zone
DSTF	Dead Sea Transform Fault
MCTF	Main Caucasus Thrust Fault
NTF	North Tabriz fault
MMF	Main Marmara Fault
CF	Chalderan fault
AG	Aegean
HT	Hellenic Trench
AN	Anatolian
NU	Nubian
AR	Arabian
EU	Eurasian
LU	Lut
CI	Central Iran block
KA	Kavir
AL	Alborz
CA	Caucasus
BS	Black Sea
SIN	Sinai
SWAN	Southwest Anatolian
SEAG	Southeast Aegean
CGR	Central Greece
NGR	Northern Greece
MAR	Marmara
CMT	Centroid Moment Tensor
IGS	International GNSS Service
USGS	United States Geological Survey

[1] Shanghai Astronomical Observatory, Chinese Academy of Sciences, Shanghai 200030, China. E-mail: sgjin@shao.ac.cn

[2] University of Chinese Academy of Sciences, Beijing 100049, China.

[3] Institute of Geology and Geophysics, Azerbaijan National Academy of Sciences, 1143 Baku, Azerbaijan.

[4] School of Earth and Space Sciences, Peking University, Beijing 100871, China.

1. Introduction

The Eastern Mediterranean and Caucasus are located between the African, Arabian and Eurasian Plates, with complicated tectonic activity connected with the Anatolian, Nubian and Somalian major lithospheric plates (McKenzie 1970, 1972). The Caucasus, Bitlis-Zagros and eastern Anatolian are active continental collision zones due to the present-day tectonic settings of the region (Fig. 1). The Eastern Mediterranean is a hazardous area that can aid in understanding fundamental tectonic processes such as passive margins, continental rifting, subduction and accreditation (Robertson and Mountrakis 2006). These general processes have been studied for extensive areas of the continental lithosphere to determine whether the region is undergoing aseismic deformation. Crustal deformation research contributes beneficial information regarding continental deformation.

The study region has experienced various catastrophic earthquakes throughout its recorded history. Earthquake activity was seen around the Aegean Sea, comprising a large part of Greece, and western Anatolia has had the most remarkable geodynamic processes in the region. The tectonic development of the area is dominated by the impacts of subduction along the Hellenic arc and continental collision in eastern Turkey and Caucasus. Aegean and western Turkey is a continuation of the continental crust of the northward subduction zone of the African Plate (McClusky et al. 2000, 2003). Regarding historical seismicity, large earthquakes with magnitudes of $M_w \geq 6$ have occurred in the study region. The concentrated seismic and tectonic motions of the Anatolian Plate largely determine the strain and slip rates in the Marmara region, western and central Anatolian region, and along the North Anatolian Fault Zone (NAFZ) (Reilinger et al. 1997; Aktug et al. 2013). McKenzie (1970) reported that the adjustment of the Dead Sea Transform fault (DSTF) did not match the assumed direction of a transform fault between the Nubian and Arabian Plates. The author proposed the existence of the Sinai sub-plate, which causes the transcurrent movement of the Arabian–Nubian along the DSTF. However, the detailed slip rates and locking depths along the main faults in the region are still not precise due to shorter or fewer GPS observations.

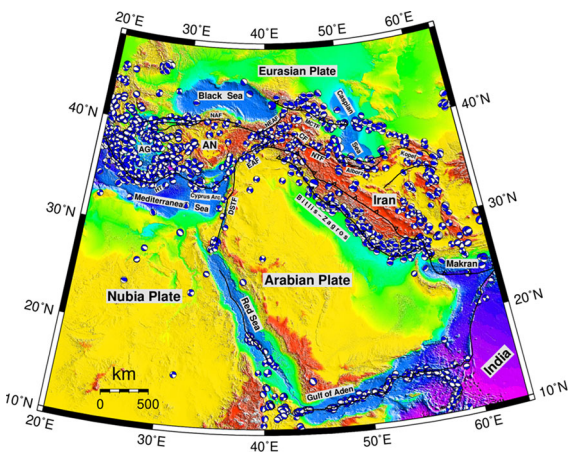

Figure 1
Simplified tectonic and topographic/bathymetric (SRTM30 plus) map of the study area, including the zone of interaction of the Nubian, Arabian, Anatolian and Eurasian plates. Abbreviations: North Anatolian Fault Zone (NAFZ), East Anatolian Fault Zone (EAFZ), Dead Sea Transform fault (DSTF), North Tabriz fault (NTF), Chalderan fault (CF), Aegean (AG), Main Caucasus Thrust Fault (MCTF), Hellenic Trench (HT), Anatolian (AN). Focal mechanisms for earthquakes in the study area are from the Global CMT Catalog (1976–2017)

GPS has provided new possibilities to assess the present-day plate motions and deformations directly (e.g., Hager et al. 1991). Previous GPS studies have quantified regional deformation in the plate interaction zone in the study region (Ahadov and Jin 2017; Bayer et al. 2006; Masson et al. 2007; Wdowinski et al. 2004; Aktug et al. 2009, 2013; Alchalbi et al. 2010; Reilinger et al. 1997, 2006; McClusky et al. 2000, 2003; Le Pichon et al. 1995; Meade et al. 2002; Mahmoud et al. 2005; Le Beon et al. 2008; Vernant 2015). The regional plate motion studies used fault orientation, local observations and constraints from the relative plate motion. The main disadvantages in the region present-day deformation are poorly constrained. Thus, the individual segments do not take into account the strain of the entire plate boundary. Previous GPS studies have used limited data along the main faults. In this case, it was not possible to define the slip rate and locking depth for the different segments as a result of the unequal distribution of geodetic stations. In this article, we used intensive GPS field data to create a new block model. The slip rate, locking depth and moment rate for the different

profiles along the main faults in the region are estimated and investigated from the velocity fields of more than 1000 continuous GPS (CGPS) and survey-mode GPS (SGPS) stations.

2. Regional Tectonic Setting

The Eastern Mediterranean is located among three main tectonic plates, namely the Arabian, Nubian, and Eurasian. Oceanic collision occurs in the Hellenic and Cyprus Arcs between the Nubian and Anatolian Plates as a result of the interaction of the Arabian and African Plates with the Eurasian Plate (McKenzie 1972; Jackson and McKenzie 1984). The seismic activity of Turkey is different from that of Iran due to the occurrence of significant earthquakes in the area far from the three belts. The major tectonic structures in the Central Anatolian Region (CAR) consist of intraplate strike-slip faults and pull-apart basins. Although Central Anatolia has been observed as a deformation-free area in many investigations, the Anatolian and surrounding regions incorporate a wide diversity of tectonic phenomena including transform strike-slip faulting, continental collision and main thrust faulting, subduction, contraction, extension and various comparatively small-scale processes (McKenzie 1972; Jackson and McKenzie 1984; Barka and Reilinger 1997; Öztürk 2020).

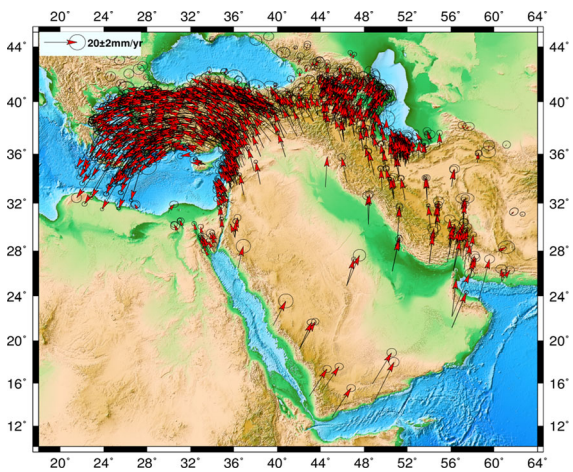

Figure 2
GPS velocities with 95% confidence ellipses in the Eurasian Plate fixed frame

Anatolian Plate motion is driven by the push of the Arabian Plate in the east and the subduction along the Hellenic arc in the south-west (Le Pichon and Angelier 1979; Jackson and McKenzie 1984). The NAFZ describes the northern edge of the Anatolian Plate with the Eurasian Plate and is the dominant strike-slip fault (Barka and Kadinsky-Cade 1988). The East Anatolian Fault Zone (EAFZ) places the boundary between the Arabian and Anatolian Plates. The EAFZ is well observed with a strike-slip fault system. The collision of the Arabian with the Eurasian Plate exhibits shortening in the region of the lithosphere. This shortening is probably due to the lateral transformation associated with the thickening of the lithosphere (McKenzie 1972). Usually considered a conjugate structure to the NAFZ, the EAFZ is a $\sim$ 600 km-long SW-NE trending fault zone between the north and the south (McKenzie 1970). The EAFZ is considered a continuation of the DSTF to the north, where the subduction of the African Plate under the Anatolian Plate and the differential motion of the Arabian Plate relative to the African Plate are the main driving mechanisms (McKenzie 1972; Şengör and Kidd 1979).

The Caucasus is located in the continental collision zone between the Arabian and Eurasian Plates. At the longitude of Iran, most of the $\sim$25 mm/year shortening between the Arabian and Eurasian Plates occurs within three major deformation belts: the Zagros Mountains in the south, the Alborz mountains on the southern border of the South Caspian Basin, and the trans-Caspian Absheron–Balkhan sill in the north. The southern belt follows the Zagros range close to the northern boundary of the Arabian Plate. GPS data indicate that the velocity of the South Caspian Basin relative to the Eurasian Plate is 6 ± 2 mm/year and the motion across the central Alborz is about 5 ± 2 mm/year in shortening and 4 ± 2 mm/year (Vernant et al. 2004). The active faults and earthquake source mechanisms surrounding the basin are estimated to be NW relative to the Eurasian Plate and southwestern Iran (Jackson et al. 2002).

The Arabian–Nubian is a divergent margin in the Red Sea into the convergence movement between the Eurasian and Arabian by extrusion of the Anatolian Plate. The southwestern boundary between Nubia and

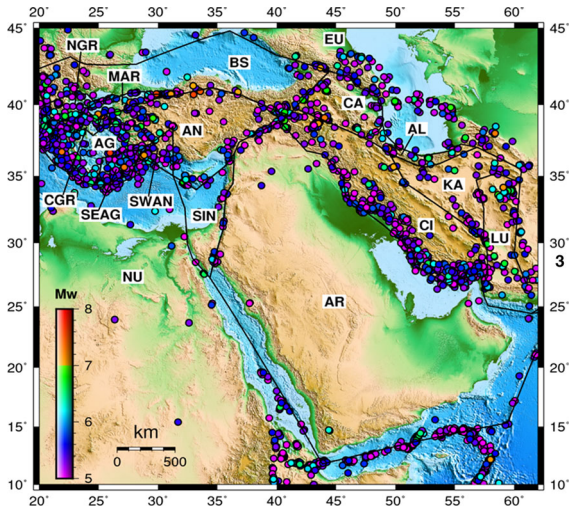

Figure 3
Map showing block model consisting of 15 plates/blocks and $M_w \geq 5$ earthquakes (USGS; 1960–2017). Black lines show defined block boundaries from Reilinger et al. (2006). Abbreviations: Nubian (NU), Arabian (AR), Eurasian (EU), Anatolian (AN), Aegean (AG), Lut (LU), Central Iran block (CI), Kavir (KA), Alborz (AL), Caucasus (CA), Black Sea (BS), Sinai (SIN), south-west Anatolian (SWAN), south-east Aegean (SEAG), central Greece (CGR), northern Greece (NGR), Marmara (MAR)

Sinai of the divergent movement in the Red Sea turns into the Gulf of Suez. Seismic activity extends over a large area to the north of the Dead Sea, reflecting the destruction of northern Israel and Lebanon. The north-west region of the Arabian Plate incorporates several active tectonic elements including the DSTF, the Arabian-Eurasian continental collision in southern Turkey (Bitlis-Zagros fold-thrust belt), the intracontinental Palmyride fold-thrust belt and the Euphrates depression.

3. Data and Modelling Method

In this paper, we used combined dense GPS data from Ahadov and Jin (2017). All GPS data have at least 5 years of observations, and more than 1000 GPS velocities are obtained from survey-mode GPS (SGPS), continuous GPS (CGPS) and International GNSS Service (IGS) stations. GPS velocities are shown in the Eurasian Plate fixed reference frame (2σ error ellipse indicates 95% confidence ellipses, Fig. 2). We have modelled crustal deformation using the elastic block approach. Block models of crustal deformation support the analysis and simultaneous interpretation of various types of data that are related to motions of the block and slip rates on faults. In this

Table 1
GPS-Euler rotation rate relative to Eurasia and 1σ uncertainties (For abbreviations, see Fig. 3)

Block	Fixed	Longitude (°)	Latitude (°)	Ω (°/Myear)	σ	WRMS
CA	EUR	37.68	41.52	0.78	0.08	1.40
AR	EUR	24.11	23.65	0.42	0.11	1.60
AL	EUR	60.94	37.45	− 0.66	0.11	1.20
KA	EUR	88.18	38.06	− 0.22	0.08	0.67
CI	EUR	128.35	11.83	0.12	0.08	1.64
AN	EUR	32.66	31.62	1.31	0.17	1.38
MAR	EUR	29.49	34.96	1.87	0.28	2.95
SIN	EUR	11.22	8.15	0.15	0.07	0.29
SWAN	EUR	31.61	34.71	3.52	0.47	2.57
AG	EUR	37.22	29.33	1.26	0.13	3.41
BS	EUR	30.81	27.92	0.17	0.03	3.48
SEAG	EUR	157.04	41.08	0.44	0.24	2.47
AL	CA	48.79	40.21	1.44	0.10	
KA	CA	48.02	42.67	0.95	0.09	
CI	CA	49.29	42.34	0.81	0.07	
CA	AR	61.33	56.87	0.42	0.12	
AL	AR	45.57	33.47	1.05	0.02	
KA	AR	41.77	31.67	0.57	0.03	
CI	AR	42.06	27.36	0.42	0.04	
CA	AL	48.79	40.21	1.44	0.10	
KA	AL	50.17	35.41	0.49	0.02	
CI	AL	48.21	37.50	0.63	0.02	
CA	KA	48.01	42.67	0.95	0.09	
AL	KA	50.17	35.41	0.49	0.02	
CI	KA	40.75	44.22	0.15	0.02	
CA	CI	49.29	42.34	0.81	0.07	
AL	CI	48.21	37.50	0.63	0.02	
KA	CI	40.75	44.22	0.15	0.02	
AN	AR	37.14	35.17	0.89	0.07	
MAR	AR	34.33	36.30	0.76	0.08	
SIN	AR	31.93	31.10	0.29	0.04	
SWAN	AR	32.75	36.16	3.10	0.38	
AG	AR	39.23	33.68	1.22	0.07	
BS	AR	20.16	20.75	0.26	0.08	
SEAG	AR	2.67	34.82	0.81	0.32	
MAR	AN	51.58	27.76	0.14	0.02	
SWAN	AN	30.96	36.52	2.21	0.31	
AG	AN	44.59	29.41	0.33	0.02	
BS	AN	32.95	32.17	1.14	0.14	
SEAG	AN	20.78	36.25	1.65	0.39	
MAR	AG	46.67	28.96	0.46	0.04	
SWAN	AG	28.41	37.56	1.90	0.31	
SEAG	AG	24.91	35.46	1.95	0.38	
AN	BS	32.95	32.17	1.14	0.14	
MAR	BS	30.34	32.55	1.01	0.15	

paper, we applied the McCaffrey (2002) approach, where all the Euler rotations of the micro-blocks are simultaneously determined by reducing the misfit of the velocities. The surface deformation caused by fault slip over small, finite-fault patches between the nodes, with bilinear interpolation, is used to estimate slip magnitude at every patch (McCaffrey 2002, 2009). McCaffrey (2002) aimed to combine block rotations with the half-space dislocation models that determine strain near locked faults. Rotation poles for blocks describe both the rigid block movements and the average relative slip along the block boundary.

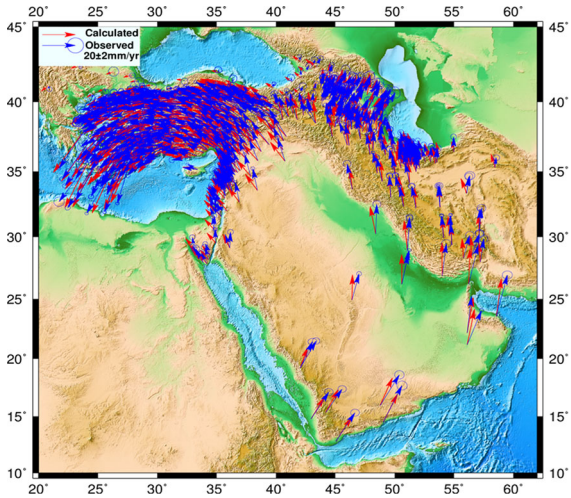

Figure 4
Compared calculated surface velocities with observed velocities

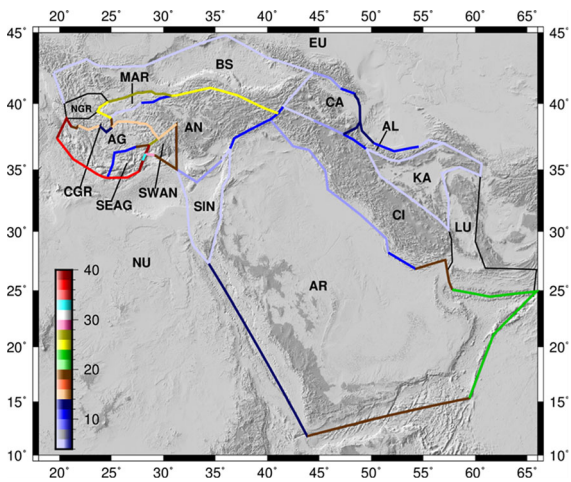

Figure 5
The map shows the slip rate along the plate boundaries, color-coded by slip rate

Figure 6 ▶
The individual velocity fields were used in the analysis (top). The velocity profiles with slip rate and locking depth of the NAFZ estimated simultaneously (bottom). The red curve shows the best-fit model to the GPS data (with error bars at 95% confidence level)

We have used a geodetic modelling program called Tdefnode (McCaffrey 2002, 2009). Tdefnode allows us to analyse deformation transients as well as block motions. Tdefnode uses GPS velocity data and fault geometry to predict rotation rates of blocks, slip rates, and locking extent. The program later splits the region into fault-bounded elastic blocks. It then predicts its surface velocities using specific modelled parameters. The program compares its modelled surface velocities with observed surface velocities and selects the set of parameters that reduce the variance between the two (McCaffrey 2002). Relative block motion is quantified by angular velocities that in turn define fault slip vectors as a function of position along the fault. Fault slip rates are dependent on the difference in velocity of points on opposite sides of fault boundaries. This definition uses the second way to estimate the fault slip rate (McCaffrey 2002). The faults that separate the domains are represented by nodes assigned on their surfaces. The value of φ at every node is then calculated while the fault slip vector V is calculated from the adjacent angular velocities. By dividing the dots on the defective surface into smaller patches and using bilinear interpolation between the points, we obtain φV smooth coupling over the defect. In the elastic hemisphere dislocation model, surface velocities are compared to the amount of φV called slip velocity deficiencies. We combine the fault surface between the fault nodes by dividing it into small patches and using bilinear interpolation between nodes to produce a smooth combination of φV on the fault (McCaffrey 2002).

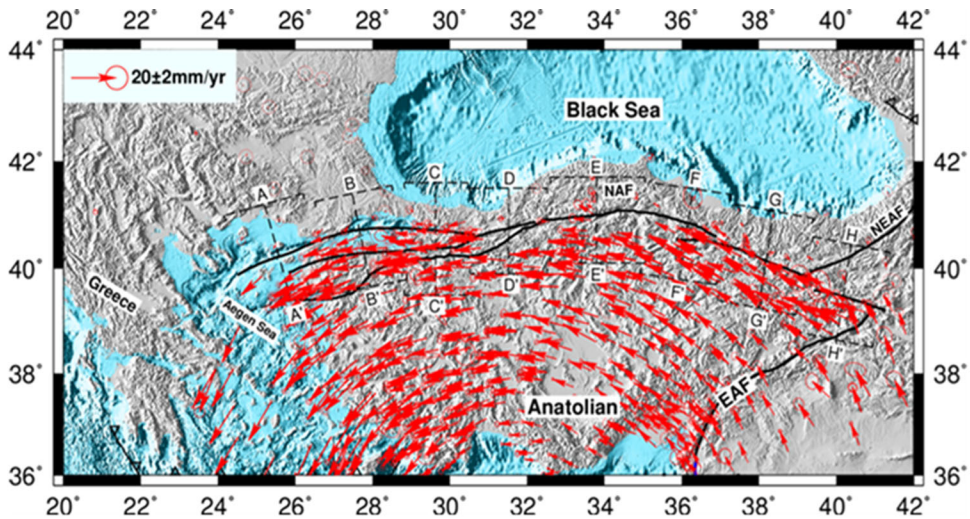
20±2mm/yr
Black Sea
Anatolian
Greece
Aegean Sea
NAF
NEAF
EAF
A
B
C
D
E
F
G
H
A'
B'
C'
D'
E'
F'
G'
H'
20°
22°
24°
26°
28°
30°
32°
34°
36°
38°
40°
42°
44°

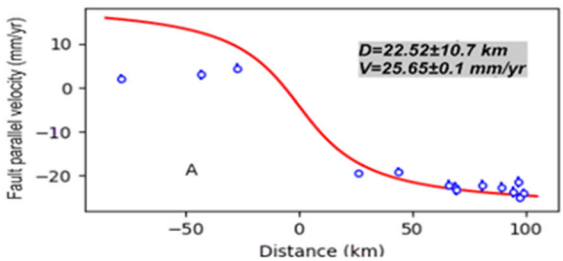
D=22.52±10.7 km
V=25.65±0.1 mm/yr
A
Fault parallel velocity (mm/yr)
Distance (km)

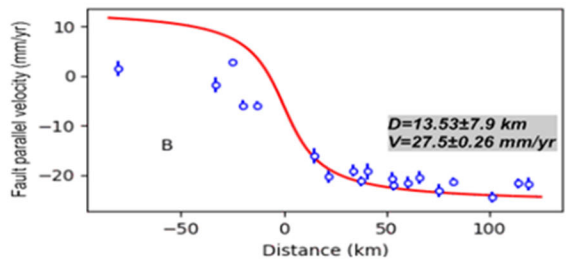
D=13.53±7.9 km
V=27.5±0.26 mm/yr
B
Fault parallel velocity (mm/yr)
Distance (km)

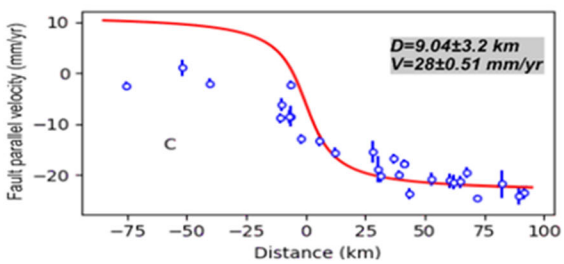
D=9.04±3.2 km
V=28±0.51 mm/yr
C
Fault parallel velocity (mm/yr)
Distance (km)

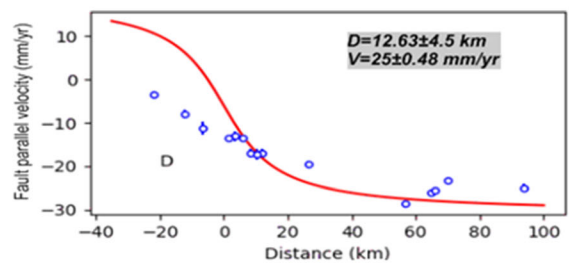
D=12.63±4.5 km
V=25±0.48 mm/yr
D
Fault parallel velocity (mm/yr)
Distance (km)

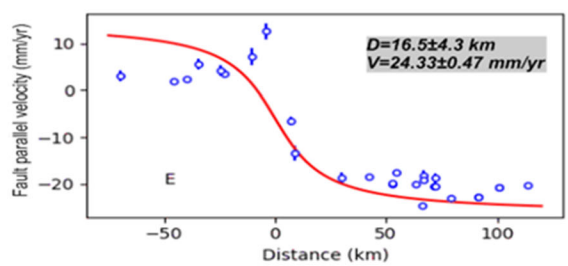
D=16.5±4.3 km
V=24.33±0.47 mm/yr
E
Fault parallel velocity (mm/yr)
Distance (km)

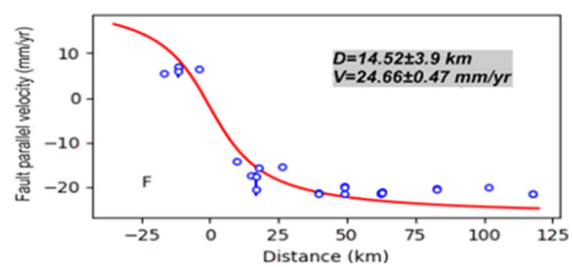
D=14.52±3.9 km
V=24.66±0.47 mm/yr
F
Fault parallel velocity (mm/yr)
Distance (km)

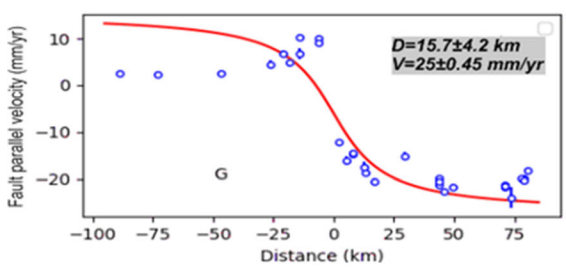
D=15.7±4.2 km
V=25±0.45 mm/yr
G
Fault parallel velocity (mm/yr)
Distance (km)

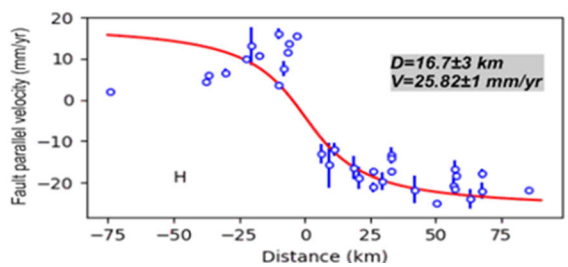
D=16.7±3 km
V=25.82±1 mm/yr
H
Fault parallel velocity (mm/yr)
Distance (km)

4. Results and Discussion

4.1. Rigid-Block Modelling

The surface of the Earth consists of a group of stable tectonic plates rotating slowly above the mantle, with deforming zones placed near plate boundaries. Previous studies (e.g., DeMets et al. 1990, 2010; Bird 2003; Altamimi et al. 2011; Argus et al. 2011; Kreemer et al. 2014; Ahadov and Jin 2017) have better defined the extent of small tectonic blocks and solid crustal blocks within these deforming zones. Several observed GPS velocity fields can be modelled by rigid rotating blocks that are strained near their borders due to interactions with other blocks opposite the bounding faults. The preferred block model and seismicity of the region are shown in Fig. 3

Euler rotation rates have been determined from GPS data for the Arabian, Anatolian, Caucasus Plates and small blocks relative to the Eurasian Plate (Table 1).

GPS velocities with uncertainties lower than 2 mm/year were used to estimate absolute rotation poles of 12 tectonic plates/blocks. The relative Euler rotation rates determined between the Arabian–Eurasian, Anatolian–Eurasian, Caucasus–Eurasian and Central Iranian Euler are 0.42 ± 0.1 deg/Myear, 1.31 ± 0.017 deg/Myear, 0.78 ± 0.08 deg/Myear and 0.12 ± 0.08 deg/Myear. McClusky et al. (2000) and Reilinger et al. (2006) concluded a kinematic model of the region with a relative rotation of small blocks. The angular velocity field shows both counterclockwise and clockwise rotation. The counterclockwise rotation is determined in the Arabian and Anatolian Plates and the Caucasus and Central Iranian blocks, while clockwise rotation is seen in the Alborz and Kavir blocks. Our results for orientation of relative motion agree with predicted GPS velocities. The Arabian-Eurasian convergence is accommodated in northern Iran and Caucasus.

4.2. Slip Rate

The estimation of slip rates from dense observations is very sensitive to preventing possible locking depths and spatial density of data. The lack of sufficient data near block boundaries and the rigid parts of the blocks typically occurs in a high correlation of parameters such that the elastic strain accumulation cannot be rigorously distinguished from the rigid. Moreover, the trade-off between slip rate and locking depth largely depends on the network coverage and the spatial density. We compared our calculated surface velocities with observed velocities (Fig. 4). Observed velocities are the only measurements of known quantity other than fault geometry in our model. Our calculated velocities are in good agreement with those observed by GPS, which encourages us to proceed with further results from the model, such as slip rates.

The NAFZ is dominated by the right-lateral strike-slip with extension in the Marmara. Estimated geodetic slip rates along the Main Marmara Fault (MMF) vary significantly between 17 and 28 mm/year. Previous GPS-constrained models predicted right-lateral MMF slip rates of 23, 24.4–24.8 and 24.6–27.9 mm/year, respectively (Le Pichon et al. 2003; Meade et al. 2002; Reilinger et al. 2006). Our slip rates range between 24 and 28 mm/year along the NAFZ (Fig. 5). We assume that full relative plate motion of the Anatolian Plate with respect to the Eurasian Plate has to define the slip rate on the MMF.

Block modelling assumes the rotation to be the same inside the block, but the slip rate may change along the plate boundaries. However, the slip rates along an extended fault system can vary depending on elasticity variations, even if the derived velocity is constant (Chéry 2008). Reilinger et al. (2006) reported 25.8 ± 0.2 and 25.3 ± 0.2 mm/year slip rates for profiles F and G. Aktuğ et al. (2015) found a slip rate of 22.8 ± 0.4 mm/year by using the block modelling approach for profiles F and G, respectively. The block model computed slip rates of 24.66 ± 0.47 mm/year and 25 ± 0.45 mm/year by using the block modelling approach for profiles F and G (Fig. 6). The slip rate in the central part of the NAFZ located to the west of the study area was estimated to be in the range of 19–21.5 mm/year (Yavaşoğlu et al. 2011), while the slip rate was estimated in the range of 16–24 mm/year to the east of the NAFZ (Ozener et al. 2010). The GPS-derived slip rates of the central NAFZ calculated in this study for profiles D, E and F are 25 ± 0.48 mm/year,

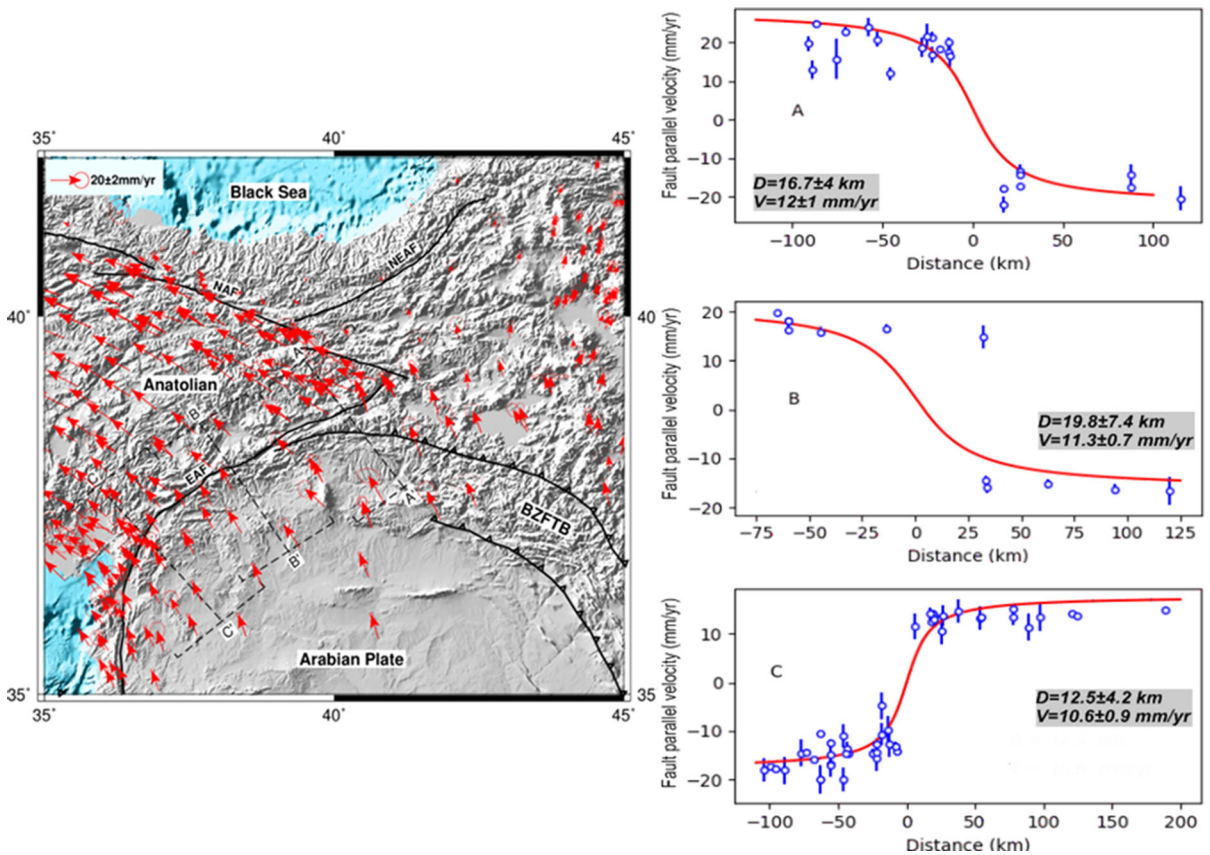

Figure 7
The individual velocity fields were used in the analysis (left). The velocity profiles with slip rate and locking depth estimated simultaneously of the EAFZ (right). The red curve shows the best fit model to the GPS data (with error bars at 95% confidence level)

24.33 ± 0.47 and 24.66 ± 0.47, respectively (Fig. 5).

In previous studies, the relative motion between the Anatolian and Arabian Plates was determined using regional GPS networks. Crustal deformation was associated with the EAFZ and DSTF systems. Geodetic measurements showed a slip rate of 11 mm/year based on the relative rotations of these large blocks (Reilinger et al. 1997; McClusky et al. 2000). Our estimated slip rates agree with the earlier studies, while our denser data set and assumed block geometry allow us to constrain the slip rates of the individual profiles of the EAFZ and DSTF faults. The detailed left-lateral slip rate is estimated to be ~ 11.3 ± 0.8 mm/year along the EAFZ. A previous study (Aktuğ et al. 2013) observed the largest slip rate to be 13 mm/year, decreasing to 7.5 mm/year in the northern part of the Karliova Triple Junction (KTJ). In comparison, Aktug et al. (2016) found that the left-lateral slip rates ranged between 10 and 12 mm/year from the north to the south along the EAFZ. Earlier GPS data revealed a continuous variation of 4.5 mm/year along the southern segment (Mahmoud et al. 2005) and 2 mm/year in the northern part (Alchalbi et al. 2010). We found that the left-lateral slip rate along the EAFZ changes from 10 to 12 mm/year, while the left-lateral slip rate of the DSTF is 4–5 mm/year (Fig. 5). The geodetic slip rate is similar to the long-term estimate of 3.3–4.0 mm/year reported by Gomez et al. (2007) based on an evident displacement in NW Syria. Le Beon et al. (2008) reported the present-day deformation in the southern segment of the DSTF on the basis of new GPS data in Israel and Jordan. The horizontal

Table 2

The estimation of the slip rates and the locking depth

Faults	Profiles	V (mm/year)	D(km)
NAFZ	A	25.65 ± 0.1	22.52 ± 10.7
	B	27.5 ± 0.26	13.53 ± 7.9
	C	28 ± 0.51	9.04 ± 3.2
	D	25 ± 0.48	12.63 ± 4.5
	E	24.33 ± 0.47	16.5 ± 4.3
	F	24.66 ± 0.47	14.52 ± 3.9
	G	25 ± 45	15.7 ± 4.2
	H	25.82 ± 1.05	16.7 ± 3
EAFZ	A	12 ± 1	16.7 ± 4
	B	11.3 ± 0.7	19.8 ± 7.4
	C	10.6 ± 0.9	12.5 ± 4.2
DSTF	A	5 ± 1.02	10.9 ± 5.5
	B	4.3 ± 0.75	9 ± 4
	C	4.1 ± 0.95	11.8 ± 6.7
MCT	A	6.5 ± 0.2	12.7 ± 5.8
	B	8.2 ± 0.6	14.2 ± 4
	C	10.3 ± 0.6	16.5 ± 3.3
	D	14.3 ± 0.7	17.8 ± 4.9

The results of the profile parameters D (depth) and V (slip rate) and uncertainties

velocity field relative to the Arabian is well defined and presents left-lateral motion on the fault, providing a best-fit slip rate of 4.9 ± 1.4 mm/year.

The Arabian-Eurasian convergence zone is an active continental collision in the east of Turkey and the Lesser Caucasus, lateral transport of lithosphere out of the region of plate convergence and shortening along the Main Caucasus Thrust Fault (MCTF). Previous studies (Kadirov et al. 2008, 2015) have measured the present-day slip rate using GPS along the MCTF. The estimated slip rate along the MCTF range between 4–10 mm/yr from westward to eastern Azerbaijan. However, the small number of GPS stations in the region and the lack of data along the block boundary are a significant limitation. In this instance, the use of the block model to determine slip rates on the different profiles is challenging due to the unequal distribution of geodetic stations. We used a denser GPS data set and assumed block geometry, which allowed us to constrain the slip rates of the different segments of the main faults. Our detailed block model showed slip rates of 14.3 ± 0.7 mm/year for the eastern MCTF and 6.5 ± 0.2 mm/year for the western MCTF (Fig. 5).

4.3. Locking Depth

For an infinitely long vertical strike-slip fault, the classical relationship (Savage and Burford 1973) between the fault-parallel velocities and distance to the fault is given by

$$v = \frac{V}{\pi}\tan^{-1}\left(\frac{x}{D}\right), \quad (1)$$

where x is the perpendicular distance to the fault, V is the slip rate, D is the locking depth, and v is station velocity. According to this two-dimensional model, the uppermost portion of the fault locked due to friction between earthquakes, whereas the lower part creeps continuously at a constant rate equal to the speed of the relative plate motion.

4.3.1 North Anatolian Fault Zone (NAFZ)

Many researchers have found that the locking depth for the eastern part of Marmara ranges between 10 and 15 km based on GPS and seismological data. Meade et al. (2002) observed recoverable elastic strain accumulation in the Marmara region using a block model and found that the GPS data was best explained by a shallow locking depth (5–6 km) on the EW-trending direct fault in the Marmara Sea. The results reported by Ergintav et al. (2009) also support a shallow locking depth in the eastern part of the Marmara Sea. Our results (Fig. 6) show that the fault locking depth for profiles B and C are 13.5 ± 7.9 km and 9 ± 3.2 km in the MMF, respectively. Yavaşoğlu et al. (2011) estimated a locking depth of 16 km with uncertainty of 6 to 20 km in the central part of the NAFZ. Our estimated locking depth (Profile E) is 16.5 ± 4.3 km using dense GPS data. Peyret et al. (2012) applied the InSAR technique using ENVISAT and ERS data in the same region and observed a locking depth range between 15 and 20 km. Walters et al. (2011) studied the same segment with InSAR and found that the locking depth ranged between 13.5 and 25 km in the easternmost part of the NAFZ. Aktuğ et al. (2015) calculated locking depths of 12.6 ± 2.4 km and 12 ± 3.5 km for the same profiles. Tatar et al. (2012) studied the GPS data for the F and G profiles and found that the fault locking depth increased westward from 8.1 ± 3.3 to 12.8 ± 3.9 km. We

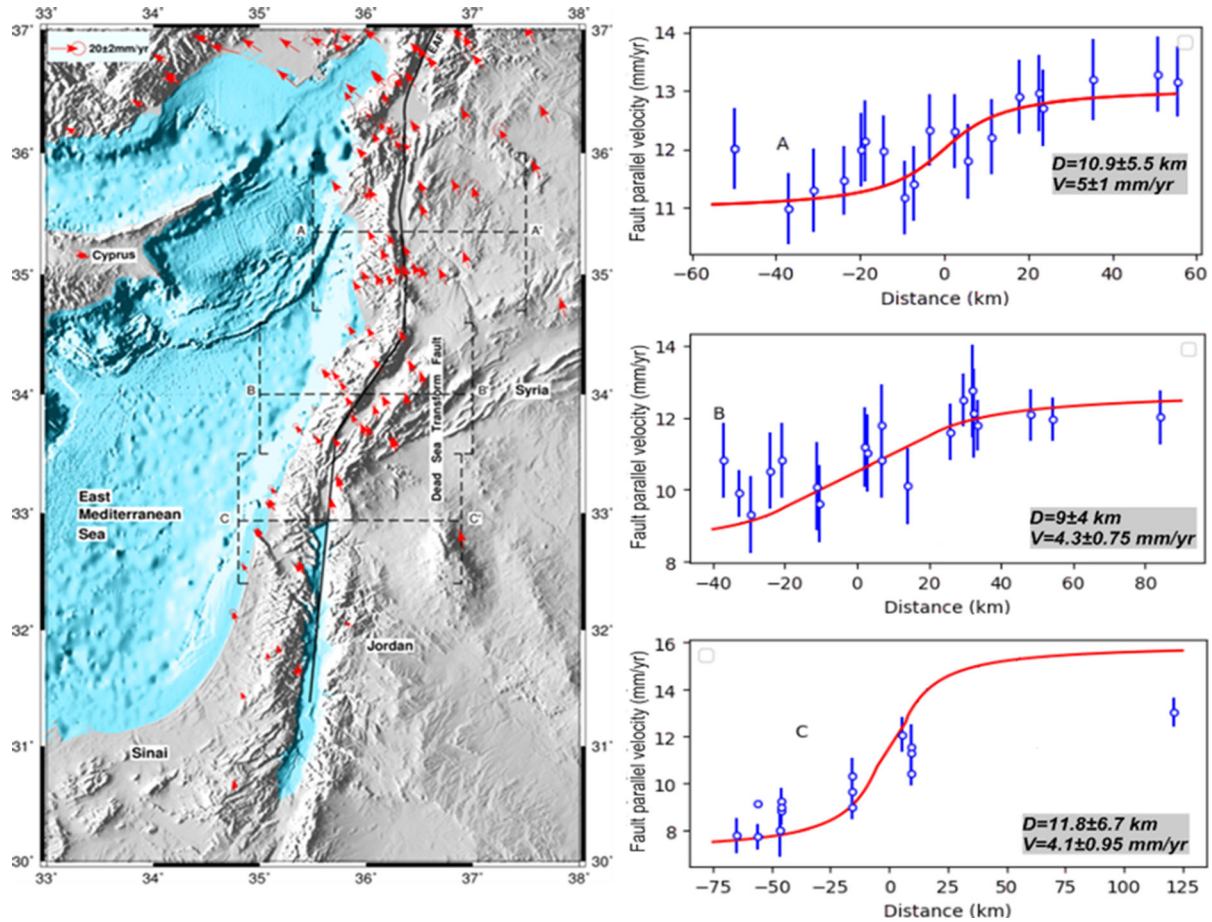

Figure 8
The individual velocity fields were used in the analysis (left). The velocity profiles with slip rate and locking depth estimated simultaneously of the DSTF (right). The red curve shows the best fit model to the GPS data (with error bars at 95% confidence level)

computed locking depths of 14.52 ± 3.9 km and 15.7 ± 4.2 km for the same profiles, respectively. For the shallow locking depth in the MMF (9 ± 3.2 km), the westernmost part of MMF has a deeper locking depth (22.5 ± 10.7 km), with high uncertainty. This high uncertainty is explained by fewer station data and fault geometry.

4.3.2 East Anatolian Fault Zone (EAFZ)

Cavalié and Jónsson (2014) estimated a much shallower locking depth from InSAR that was ∼ 4.5 km in the EAFZ, suggesting that this part of the fault creeps almost free to the surface. Aktug et al. (2016) assumed a locking depth of 25 ± 6.25 km for the middle segment. Our results (Fig. 7) are 16.7 ± 4.4 km in the northern section, 19.8 ± 7.4 in the central part and 12.5 ± 4.2 km in the southern profile along the EAFZ (Table 2).

4.3.3 Dead Sea Transform Fault (DSTF)

Geodetic locking depths for the DSTF range from 9 to 12 km, and uncertainties are typically about 4 to 7 km. In general, elastic dislocation models have a reasonable correlation with long-term slip rates, along with other significant strike-slip faults in the region, as well as the southern and central DSTF (e.g. Mahmoud et al. 2005; Reilinger et al. 2006; Gomez et al. 2007; Le Beon et al. 2008). Nevertheless, more detailed information on the velocity field proves that the velocity changes along the strike. Le Beon et al.

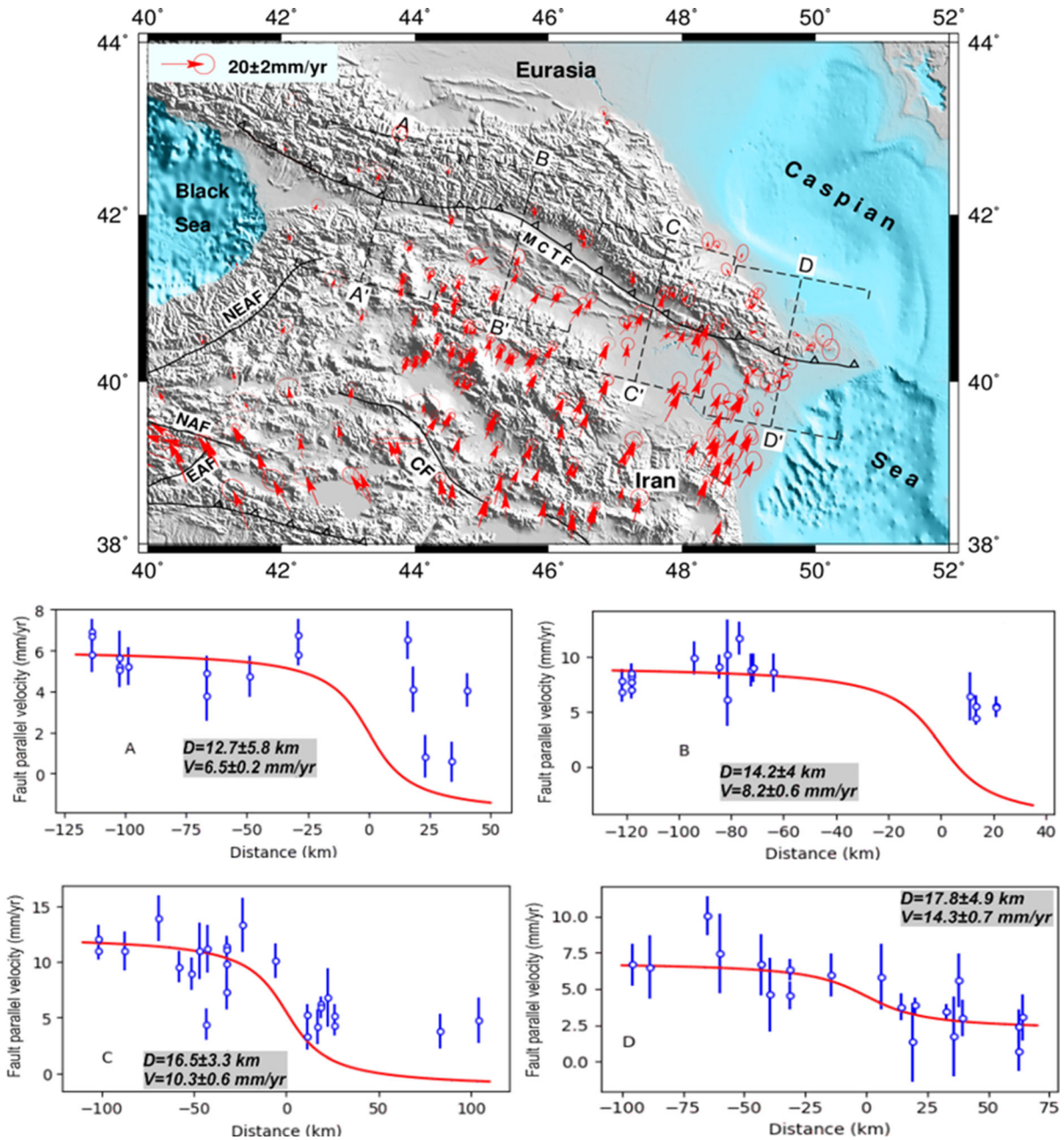

Figure 9
The individual velocity fields were used in the analysis (top). The velocity profiles with slip rate and locking depth of the MCTF (bottom) estimated simultaneously. The red curve shows the best-fit model to the GPS data (with error bars at 95% confidence level)

(2008) observed a locking depth of 11 ± 9 km in the southern DSTF applying a different method and different data, but difficulty in estimating locking depth along the northern segment (Alchalbi et al. 2010; Mahmoud et al. 2013). Our geodetic locking depth results (Fig. 8) from dense GPS data are 10.9 ± 5.5 km in the northern profile, 9 ± 4 km in the central profile and 11.8 ± 6.7 km along the DSTF (Table 2). Gomez et al. (2007) assumed a fault locking depth of 15 km, while Masson et al.

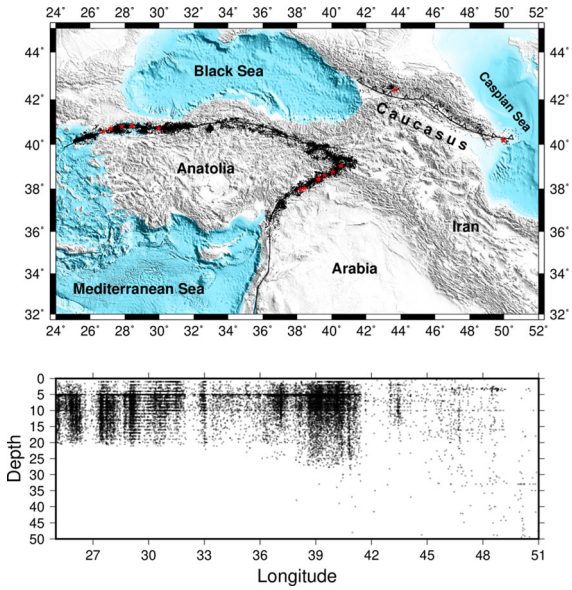

Figure 10
Seismic activity along the main active faults. Seismic activity as a function of time showing that seismicity occurs regularly along the segments (red stars show $M_w \geq 6$ earthquakes)

(2015) estimated a locking depth of 14.5 ± 4.1 km in the southern part of the DSTF, which is very similar to the results proposed earlier by Le Beon et al. (2008).

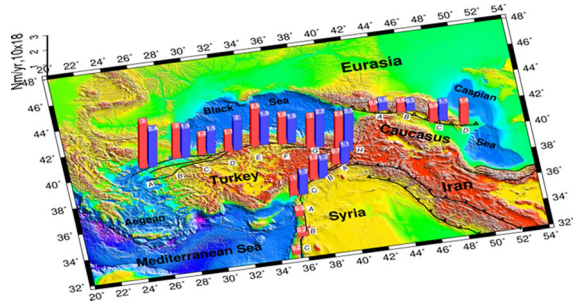

Figure 11
Seismic moment rate derived from geodetic locking depth (red) and seismogenic depth (blue)

4.3.4 Main Caucasus Thrust Fault (MCTF)

Seismological observations show that the north-dipping thrust faults along the southern border of the western and central Greater Caucasus are seismically active. The depth of the shallow-dipping earthquakes is generally 10 km, but more profound events (15–20 km) were observed. The depths of earthquakes in the Caucasus obtained using teleseismic data showed that the seismogenic thickness in this region was ~ 20 km (Tan and Taymaz 2006). Our geodetic estimated locking depth results (Fig. 9) are 12.7 ± 5.8 km for the western part and 17.8 ± 4.9 km for the eastern part of the MCTF

Table 3

Estimated geodetic locking depth and seismogenic depth from this study

Faults	Profiles	V (mm/year)	Geodetic depth (km)	Seismogenic depth (km)	Geodetic M_0 10^{18} nm/year	Seismogenic M_0 10^{18} nm/year
NAFZ	A	25.65 ± 0.1	22.52 ± 10.7	15	3	2.4
	B	27.5 ± 0.26	13.53 ± 7.9	13	2	1.9
	C	28 ± 0.51	9.04 ± 3.2	13	1.2	1.5
	D	25 ± 0.48	12.63 ± 4.5	15.5	1.1	2
	E	24.33 ± 0.47	16.5 ± 4.3	12.6	2.5	1.9
	F	24.66 ± 0.47	14.52 ± 3.9	12.6	1.8	1.6
	G	25 ± 0.45	15.7 ± 4.2	17	2	2.2
	H	25.82 ± 1	16.7 ± 3	17	2.4	2.5
EAFZ	A	12 ± 1	16.7 ± 4	17	0.7	1.1
	B	11.3 ± 0.7	19.8 ± 7.4	17	1.3	1.2
	C	10.6 ± 0.9	12.5 ± 4.2	16	1	1.3
DSTF	A	5 ± 1	10.9 ± 5.5		0.3	
	B	4.3 ± 0.75	9 ± 4		0.2	
	C	4.1 ± 0.95	11.8 ± 6.7		0.2	
MCTF	A	6.5 ± 0.2	12.7 ± 5.8	14	0.4	0.5
	B	8.2 ± 0.6	14.2 ± 4	12	0.6	0.5
	C	10.3 ± 0.6	16.5 ± 3.3	19	0.9	1.1
	D	14.3 ± 0.7	17.8 ± 4.9		1.4	

(Table 2). However, our estimation has uncertainty of 3 to 6 km, depending on the density and variety of nearby geodetic observations. The difference in locking depth from 13 to 18 km is caused by several seismological and rheological parameters including the thickness of the crust and seismic activity.

4.4. Rates of Moment Accumulation

The depth of the seismic zone is an essential parameter for earthquake hazard models. Independent observations by seismology and geodesy may provide insight into the depths of faulting, but these depths do not always agree. We examined earthquake depths along the NAFZ and EAFZ from Bulut et al. (2007, 2012, 2019) and the Kandilli Observatory and Earthquake Research Institute (http://www.koeri.boun.edu.tr/sismo/2/earthquake-catalog/ KOERI, $M \geq 2$), and for the Main Caucasus Thrust Fault (MCTF) from the International Seismological Centre (http://www.isc.ac.uk/iscbulletin/search/catalogue/ ISC) catalogues between 2008 and 2017 (Fig. 10). KOERI has greatly enhanced the earthquake monitoring capability in eastern Turkey since the beginning of 2002 with the establishment of new broadband seismic stations.

We compared the locking depths assumed from geodetic models to seismogenic thickness derived from seismicity. Geodetic and seismological data contribute significantly to knowledge of the kinematics of crustal motion. The estimated slip rate from the main active faults provides useful insight into active tectonics in the study. The seismic moment accumulation rate is estimated for each fault segment of the main faults using geodetic and seismogenic locking depths.

$$\frac{M}{L} = \mu VD, \tag{2}$$

we assumed a constant shear modulus of μ = 30 GPa and used the slip rate and locking depth from Table 3.

The highest rates of seismic moment accumulation from seismicity occur along the NAFZ (Fig. 11) for the A, G and H profiles, where seismic depths are moderately deep (15–17 km). The moment rate estimates from geodesy are also highest along the A, E and H profiles. The lowest seismic moment rates are observed (1.1–1.2 $\times$ 10^{18} Nm/year) for C and D profiles of the NAFZ.

The seismic moment is a direct measurement of the strength of an earthquake caused by fault slip, and it is directly related to the stress. There is a noticeable difference between geodetic and seismogenic moment rates in profiles E and D along the NAFZ. Moreover, we observed almost the same value in segment B along the MCTF. Fault geometry and earthquake location may also play an essential role in understanding differences between seismic and geodetic locking depth. A map enables the assessment of seismic hazards in the spatial correlation between GPS analysis and seismic catalogues. This paper describes the advantages of combining GPS and seismic data to improve seismic hazard assessment along the main faults and to identify low and high potential areas for future earthquakes.

5. Conclusion

In summary, the main outcomes of this study show the different patterns of plate motion and slip rates from the dense GPS velocity field in the region. Our new findings indicate counterclockwise rotation in a wide area including the Arabian, Anatolian, and Aegean regions, the Caucasus and central Iran. The angular velocities of the Arabian Plate, Anatolian Plate, Caucasus block and Central Iranian plate with respect to the Eurasian Plate are 0.42 $\pm$ 0.11 deg/Myear, 1.31 $\pm$ 0.17 deg/Myear, 0.78 $\pm$ 0.08 deg/Myear and 0.12 $\pm$ 0.08 deg/Myear, and a clockwise rotation is observed in the Kavir and Alborz blocks. In the simultaneous estimation of the slip rates using the block model, the slip rates were found to be in the range of 24–28 mm/year along the NAFZ, 10–12 mm/year along the EAFZ, 4–6 mm/year along the DSTF and 8–14 mm/year along the MCTF. In the past, the slip rate and locking depth along the NAFZ were usually considered constant in the analyses. At the same time, our new calculations show shallow locking depth in the Marmara region at 9 $\pm$ 3.2 km, while the locking depth of the EAFZ is 16.7 $\pm$ 4.4 km in the northern segment, 19.8 $\pm$ 7.4 km in the middle segment and 12.5 $\pm$ 4.2 km in the southern segment. The locking

depths for MCTF are 12.7 ± 5.8 to 17.8 ± 4.9 km from west to east. The locking depth in the DSTF is 10.9 ± 5.5 km in the northern segment, 9 ± 6.7 km in the central segment and 11.8 ± 4 km in the southern segment. Our new block model is in good agreement with the GPS observed velocities and with reasonable fault slip rates. This new block model and comparison with seismicity present detailed kinematics of the active tectonics in the Eastern Mediterranean and Caucasus region. We also studied differences in seismic moment accumulation rate by geodesy and seismicity and found that both methods produced high rates (1.6–3 × 10^{18} Nm/year) along the NAFZ and low rates (0.2–0.6 × 10^{18} Nm/year) along the DSTF and the MCTF. The geodetic and seismic depths of the main faults showed that the maximum depths of seismicity are more consistent with the fault locking depth determined from the geodetic models.

Acknowledgements

The authors would like to thank those who made GPS velocity data available. The figures were plotted using the public domain Generic Mapping Tools (GMT) software (Wessel and Smith 1995).

Author contributions BA and SJ conceived the idea for this research. BA analysed data, produced figures and prepared the initial draft. SJ contributed to the writing of the manuscript. All authors read and approved the final manuscript.

Funding

No funding was received.

Availability of data and materials

All GPS data were collected from Ahadov and Jin (2017). Earthquakes from the background seismicity catalogues were recorded by Kandilli Observatory, Earthquake Research Institute (KOERI, http://www.koeri.boun.edu.tr/sismo), International Seismological Centre (ISC, http://www.isc.ac.uk/iscbulletin) and Bulut et al. (2007, 2012, 2019).

Compliance with Ethical Standards

Animal research (ethics) Not applicable.

Consent to publish (ethics) The authors are responsible for the reliability of the manuscript and collaborate with the Editorial Office when original pictures and data and other proof materials are required.

Clinical trials registration This article does not involve clinical trials.

Conflict of interest The authors declare that they have no competing interests.

References

Ahadov, B., & Jin, S. (2017). Present-day kinematics in the Eastern Mediterranean and Caucasus from dense GPS observations. *Physics of the Earth and Planetary Interiors, 268,* 54–64.

Aktug, B., Dikmen, U., Dogru, A., & Ozener, H. (2013). Seismicity and strain accumulation around Karliova triple junction (Turkey). *Journal of Geodynamics, 67,* 21–29.

Aktuğ, B., Doğru, A., Özener, H., & Peyret, M. (2015). Slip rates and locking depth variation along central and easternmost segments of North Anatolian Fault. *Geophysical Journal International, 202,* 2133–2149.

Aktuğ, B., Meherremov, E., Kurt, M., Özdemir, S., Esedov, N., & Lenk, O. (2013). GPS constraints on the deformation of Azerbaijan and surrounding regions. *Journal of Geodynamics, 67,* 40–45.

Aktug, B., et al. (2009). Deformation of western Turkey from a combination of permanent and campaign GPS data: Limits to block-like behavior. *Journal of Geophysical Research: Solid Earth, 114*, B10404. https://doi.org/10.1029/2008JB006000.

Aktug, B., Ozener, H., Dogru, A., Sabuncu, A., Turgut, B., Halicioglu, K., et al. (2016). Slip rates and seismic potential on the East Anatolian Fault System using an improved GPS velocity field. *Journal of Geodynamics, 94–95,* 1–12.

Alchalbi, A., Daoud, M., Gomez, F., McClusky, S., Reilinger, R., Romeyeh, M. A., et al. (2010). Crustal deformation in northwestern Arabia from GPS measurements in Syria: Slow slip rate along the northern Dead Sea Fault. *Geophysical Journal International, 180,* 125–135.

Altamimi, Z., Collilieux, X., & Métivier, L. (2011). ITRF2008: An improved solution of the international terrestrial reference frame. *Journal of Geodesy, 85,* 457–473.

Argus, D. F., Gordon, R. G., & DeMets, C. (2011). Geologically current motion of 56 plates relative to the no-net-rotation reference frame. *Geochemistry, Geophysics, Geosystems, 12,* Q11001. https://doi.org/10.1029/2011GC003751.

Barka, A., & Kadinsky-Cade, K. (1988). Strike-slip fault geometry in Turkey and its influence on earthquake activity. *Tectonics, 7,* 663–684.

Barka, A. & Reilinger, R. (1997). Active Tectonics of Eastern Mediterranean region: deduced from GPS, neotectonic and seismicity data. *Annali Di Geofisica, X2*(3), 587–610.

Bayer, R., Chery, J., Tatar, M., Vernant, P., Abbassi, M., Masson, F., et al. (2006). Active deformation in Zagros—Makran transition zone inferred from GPS measurements. *Geophysical Journal International, 165,* 373–381.

Bird, P. (2003). An updated digital model of plate boundaries. *Geochemistry, Geophysics, Geosystems, 4,* 1027. https://doi.org/10.1029/2001GC000252.

Bulut, F., Aktuğ, B., Yaltırak, C., Doğru, A., & Özener, H. (2019). Magnitudes of future large earthquakes near Istanbul quantified from 1500 years of historical earthquakes, present-day microseismicity and GPS slip rates. *Tectonophysics, 764,* 77–87.

Bulut, F., Bohnhoff, M., Aktar, M., Dresen, G. (2007). Characterization of aftershock-fault plane orientations of the 1999 İzmit (Turkey) earthquake using high-resolution aftershock locations. *Geophysical Research Letters*, *34*, L20306. https://doi.org/10.1029/2007GL031154.

Bulut, F., Bohnhoff, M., Eken, T., Janssen, C., Kılıç, T., & Dresen, G. (2012). The East Anatolian Fault Zone: Seismotectonic setting and spatiotemporal characteristics of seismicity based on precise earthquake locations. *Journal of Geophysical Research, 117,* B07304. https://doi.org/10.1029/2011JB008966.

Cavalié, O., & Jónsson, S. (2014). Block-like plate movements in eastern Anatolia observed by InSAR. *Geophysical Research Letters, 41,* 26–31.

Chéry, J. (2008). Geodetic strain across the San Andreas fault reflects elastic plate thickness variations (rather than fault slip rate). *Earth and Planetary Science Letters, 269,* 352–365.

DeMets, C., Gordon, R. G., & Argus, D. F. (2010). Geologically current plate motions. *Geophysical Journal International, 181,* 1–80.

DeMets, C., Gordon, R. G., Argus, D. F., & Stein, S. (1990). Current plate motions. *Geophysical Journal International, 101,* 425–478.

Ergintav, S., McClusky, S., Hearn, E., Reilinger, R., Cakmak, R., Herring, T., Ozener, H., Lenk, O., Tari, E. (2009). Seven years of postseismic deformation following the 1999, M = 7.4 and M = 7.2, Izmit-Düzce, Turkey earthquake sequence. *Journal of Geophysical Research: Solid Earth, 114*, B07403. https://doi.org/10.1029/2008JB006021.

Gomez, F., Karam, G., Khawlie, M., McClusky, S., Vernant, P., Reilinger, R., et al. (2007). Global Positioning System measurements of strain accumulation and slip transfer through the restraining bend along the Dead Sea fault system in Lebanon. *Geophysical Journal International, 168,* 1021–1028.

Hager, B. H., King, R. W., & Murray, M. H. (1991). Measurement of crustal deformation using the global positioning system. *Annual Review of Earth and Planetary Sciences, 19,* 351–382.

Jackson, J., & McKenzie, D. (1984). Active tectonics of the Alpine–Himalayan Belt between western Turkey and Pakistan. *Geophysical Journal International, 77,* 185–264.

Jackson, J., Priestley, K., Allen, M., & Berberian, M. (2002). Active tectonics of the south Caspian basin. *Geophysical Journal International, 148,* 214–245.

Kadirov, F. A., Floyd, M., Reilinger, R., Alizadeh, A. A., Guliyev, I. S., Mammadov, S. G., & Safarov, R. T. (2015). Active geodynamics of the Caucasus region: implications for earthquake hazards in Azerbaijan. *Proceedings of Azerbaijan National Academy of Sciences, The Sciences of Earth, 3,* 3–17.

Kadirov, F., Mammadov, S., Reilinger, R., & McClusky, S. (2008). Some new data on modern tectonic deformation and active faulting in Azerbaijan (according to Global Positioning System measurements). Proceedings Azerbaijan National Academy of Sciences. *The Sciences of Earth, 1,* 82–88.

Kreemer, C., Blewitt, G., & Klein, E. C. (2014). A geodetic plate motion and global strain rate model. *Geochemistry, Geophysics, Geosystems, 15,* 3849–3889.

Le Beon, M., Klinger, Y., Amrat, A.Q., Agnon, A., Dorbath, L., Baer, G., Ruegg, J.C., Charade, O., Mayyas, O. (2008). Slip rate and locking depth from GPS profiles across the southern dead sea transform. *Journal of Geophysical Research: Solid Earth, 113*, B11403. https://doi.org/10.1029/2007JB005280.

Le Pichon, X., & Angelier, J. (1979). The Hellenic arc and trench system: A key to the neotectonic evolution of the eastern Mediterranean area. *Tectonophysics, 60,* 1–42.

Le Pichon, X., Chamot-Rooke, N., Lallemant, S., Noomen, R., & Veis, G. (1995). Geodetic determination of the kinematics of central Greece with respect to Europe: Implications for eastern Mediterranean tectonics. *Journal of Geophysical Research: Solid Earth, 100,* 12675–12690.

Le Pichon, X., Chamot-Rooke, N., Rangin, C., Sengör, A. (2003). The North Anatolian fault in the sea of marmara. *Journal of Geophysical Research: Solid Earth, 108*, 2179. https://doi.org/10.1029/2002JB001862.

Mahmoud, S., Reilinger, R., McClusky, S., Vernant, P., & Tealeb, A. (2005). GPS evidence for northward motion of the Sinai Block: Implications for E. Mediterranean tectonics. *Earth and Planetary Science Letters, 238,* 217–224.

Mahmoud, Y., Masson, F., Meghraoui, M., Cakir, Z., Alchalbi, A., Yavasoglu, H., et al. (2013). Kinematic study at the junction of the East Anatolian fault and the Dead Sea fault from GPS measurements. *Journal of Geodynamics, 67,* 30–39.

Masson, F., Anvari, M., Djamour, Y., Walpersdorf, A., Tavakoli, F., Daignières, M., et al. (2007). Large-scale velocity field and strain tensor in Iran inferred from GPS measurements: new insight for the present-day deformation pattern within NE Iran. *Geophysical Journal International, 170,* 436–440.

Masson, F., Hamiel, Y., Agnon, A., Klinger, Y., & Deprez, A. (2015). Variable behavior of the Dead Sea Fault along the southern Arava segment from GPS measurements. *Comptes Rendus Geoscience, 347,* 161–169.

Mccaffrey, R. (2002). Crustal block rotations and plate coupling. In Stein, S., & Freynuekker, J. (Eds.) *Plate boundary zones*. Geodynamic Series 30 (pp. 101–122). Washington DC: American Geophysical Union. https://doi.org/10.1029/gd030p0101.

McCaffrey, R. (2009). Time-dependent inversion of three-component continuous GPS for steady and transient sources in northern Cascadia. *Geophysical Research Letters, 36*, L07304. https://doi.org/10.1029/2008GL036784.

McClusky, S., Balassanian, S., Barka, A., Demir, C., Ergintav, S., Georgiev, I., et al. (2000). Global Positioning System constraints on plate kinematics and dynamics in the eastern Mediterranean and Caucasus. *Journal of Geophysical Research: Solid Earth, 105,* 5695–5719.

McClusky, S., Reilinger, R., Mahmoud, S., Ben Sari, D., & Tealeb, A. (2003). GPS constraints on Africa (Nubia) and Arabia plate motions. *Geophysical Journal International, 155,* 126–138.

McKenzie, D. (1970). Plate tectonics of the Mediterranean region. *Nature, 226,* 239–243.

McKenzie, D. (1972). Active tectonics of the Mediterranean region. *Geophysical Journal International, 30,* 109–185.

Meade, B. J., Hager, B. H., McClusky, S. C., Reilinger, R. E., Ergintav, S., Lenk, O., et al. (2002). Estimates of seismic potential in the Marmara Sea region from block models of secular deformation constrained by global positioning system measurements. *Bulletin of the Seismological Society of America, 92,* 208–215.

Ozener, H., Arpat, E., Ergintav, S., Dogru, A., Cakmak, R., Turgut, B., & Dogan, U. (2010). Kinematics of the eastern part of the North Anatolian Fault Zone. *Journal of geodynamics, 49,* 141–150.

Öztürk, S. (2020). A study on the variations of recent seismicity in and around the Central Anatolian region of Turkey. *Physics of the Earth and Planetary Interiors, 301,* 106453.

Peyret, M., Masson, F., Yavasoglu, H., Ergintav, S., & Reilinger, R. (2012). Present-day strain distribution across a segment of the central bend of the North Anatolian Fault Zone from a Persistent-Scatterers InSAR analysis of the ERS and Envisat archives. *Geophysical Journal International, 192,* 929–945.

Reilinger, R., McClusky, S., Oral, M., King, R., Toksoz, M., Barka, A., et al. (1997). Global positioning system measurements of present-day crustal movements in the Arabia–Africa–Eurasia plate collision zone. *Journal of Geophysical Research: Solid Earth, 102,* 9983–9999.

Reilinger, R. et al. (2006). GPS constraints on continental deformation in the Africa–Arabia–Eurasia continental collision zone and implications for the dynamics of plate interactions. *Journal of Geophysical Research: Solid Earth, 111*, B05411. https://doi.org/10.1029/2005JB004051.

Robertson, A. H., & Mountrakis, D. (2006). Tectonic development of the Eastern Mediterranean region: An introduction. *Geological Society, London, Special Publications, 260,* 1–9.

Savage, J., & Burford, R. (1973). Geodetic determination of relative plate motion in central California. *Journal of Geophysical Research, 78,* 832–845.

Şengör, A., & Kidd, W. (1979). Post-collisional tectonics of the Turkish–Iranian plateau and a comparison with Tibet. *Tectonophysics, 55,* 361–376.

Tan, O., & Taymaz, T. (2006). Active tectonics of the Caucasus: Earthquake source mechanisms and rupture histories obtained from inversion of teleseismic body waveforms. *Geological Society of America Special Papers, 409,* 531–578.

Tatar, O., Poyraz, F., Gürsoy, H., Cakir, Z., Ergintav, S., Akpınar, Z., et al. (2012). Crustal deformation and kinematics of the Eastern Part of the North Anatolian Fault Zone (Turkey) from GPS measurements. *Tectonophysics, 518,* 55–62.

Vernant, P. (2015). What can we learn from 20 years of interseismic GPS measurements across strike-slip faults? *Tectonophysics, 644,* 22–39.

Vernant, P., Nilforoushan, F., Hatzfeld, D., Abbassi, M. R., Vigny, C., Masson, F., et al. (2004). Present-day crustal deformation and plate kinematics in the Middle East constrained by GPS measurements in Iran and northern Oman. *Geophysical Journal International, 157*(1), 381–398.

Walters, R., Holley, R., Parsons, B., Wright, T. (2011). Interseismic strain accumulation across the North Anatolian Fault from Envisat InSAR measurements. *Geophysical Research Letters, 38*, L05303. https://doi.org/10.1029/2010GL046443.

Wdowinski, S., Bock, Y., Baer, G., Prawirodirdjo, L., Bechor, N., Naaman, S., Knafo, R., Forrai, Y., Melzer, Y. (2004). GPS measurements of current crustal movements along the Dead Sea Fault. *Journal of Geophysical Research: Solid Earth, 109*, B05403. https://doi.org/10.1029/2003JB002640.

Wessel, P., & Smith, W. H. (1995). New version of the generic mapping tools. *Eos, Transactions American Geophysical Union, 76,* 329–329.

Yavaşoğlu, H., Tarı, E., Tüysüz, O., Çakır, Z., & Ergintav, S. (2011). Determining and modeling tectonic movements along the central part of the North Anatolian Fault (Turkey) using geodetic measurements. *Journal of Geodynamics, 51,* 339–343.

(Received March 16, 2020, revised December 7, 2020, accepted December 11, 2020, Published online January 8, 2021)